

Particle-in-cell/Monte Carlo simulation of a capacitively coupled radio frequency Ar/CF₄ discharge: Effect of gas composition

V. Georgieva,^{a)} A. Bogaerts, and R. Gijbels

Department of Chemistry, University of Antwerp (UIA), Universiteitsplein 1, B-2610 Wilrijk-Antwerp, Belgium

(Received 25 June 2002; accepted 9 December 2002)

A one-dimensional particle-in-cell/Monte Carlo model is developed to study a capacitively coupled radio frequency discharge in a gas mixture of argon and CF₄. The simulation takes into account the following charged particles: electrons, two kinds of positive ions (Ar⁺, CF₃⁺), and two kinds of negative ions (F⁻, CF₃⁻). The model considers electron–Ar collisions, electron–CF₄ collisions, various kinds of collisions of CF₃⁺, F⁻, CF₃⁻, or Ar⁺ with Ar or CF₄, and positive–negative ion recombination. The probability for the positive–negative ion recombination is determined from a recombination rate constant. The ion–neutral elastic and reactive collisions are simulated by an ion–molecule collision model for endothermic reactions. The typical results of this model are electron and ion densities, fluxes and energy distributions, collision rates, and electric field and potential distributions. The simulation is performed for 0.1/0.9, 0.5/0.5, and 0.9/0.1 ratios of a Ar/CF₄ mixture, as well as for pure Ar and pure CF₄ discharges at a pressure of 200 mTorr. It is observed that at high CF₄ concentration the discharge behaves as a typical electronegative discharge and that CF₃⁺ is the major positive ion. At low CF₄ concentration, keeping the other operating parameters the same, the double layer structure and the electron density maxima at the bulk–sheath interface, which are representative for an electronegative discharge, disappear and the Ar⁺ density exceeds the CF₃⁺ density by more than 1 order of magnitude. The results show that the F⁻ ions are the dominant negatively charged species for all Ar/CF₄ ratios investigated. © 2003 American Institute of Physics. [DOI: 10.1063/1.1542920]

I. INTRODUCTION

Glow discharges find an increasing application in the microelectronics industry to modify the surface properties of materials in particular for the deposition of thin films and for plasma etching of metals and semiconductors.^{1,2} Radio frequency (rf) plasma etching is well recognized for its anisotropy, which is a critical process parameter in integrated circuit manufacture,¹ and the study of this plasma processing is therefore of great interest. A variety of reactors and feedgas mixtures are used in this application. Carbon tetrafluoride CF₄ and its mixes are widely used in plasma etching of silicon and silicon dioxide.¹ In order to achieve high-resolution plasma processing it is important to understand the discharge physics and chemistry. In recent years a number of articles appeared dealing with high-density inductively coupled CF₄ and Ar/CF₄ discharges; especially diagnostic measurements and modeling.^{3–8} Maeshige *et al.*⁹ describe the design of a pulsed two-frequency capacitively coupled (cc) plasma in CF₄/Ar for sustaining a high-density plasma and discuss its ability to generate charge-free processes for producing high-aspect-ratio holes or trench etching. However, simulations and experimental data for conventional cc rf discharges in Ar/CF₄ mixtures in the open literature are very scarce.^{10,11} Rauf and Kushner¹⁰ investigated numerically the argon metastable densities in Ar/CF₄ discharges. Kaga *et al.*¹¹ present

measurements of the charged particle densities and electron energy distribution function (EEDF) and their dependences on the CF₄ content. The purpose of the present paper is a description of a model and systematic study of the plasma parameters in a conventional cc rf Ar/CF₄ discharge. The article deals with the influence of the gas composition on the discharge properties at more or less standard operating conditions. Comparison of the calculated ratio of negative ion to electron densities with the experimental data is also given.

CF₄ is an electronegative gas and its radicals play an important role in the etching process. The electron and ion densities and the electron temperature determine the production of the neutral radicals. Both experimental measurements^{12,13} and computational results^{14–16} of charged particle densities in pure cc rf CF₄ plasmas have been reported in the literature. There is a good qualitative agreement among them considering the different operating conditions. It was shown that the negative ion density in the bulk plasma exceeds the electron density by 1 order of magnitude. The abundance of negative ions is one of the main features of discharges in electronegative gases and this profoundly influences the sheath dynamics (i.e., one observes electric field reversal, double layer structure and local maxima of electron density in the sheath region).^{1,14–17}

Ar is a typical electropositive atomic gas and it is often used as an example for describing the fundamental principles of particle and energy balances in discharges.¹ Due to its relative simplicity the rf argon discharge has been studied extensively both experimentally and by computer modeling

^{a)} Author to whom correspondence should be addressed; electronic mail: vgeorg@uia.ua.ac.be

(e.g., Refs. 17–20). Discharges in electropositive gases behave differently from those in electronegative gases.¹ The contrast in the density profiles, the electric field properties, and the electron energy distribution has been the subject of several investigations.^{17,21}

The present article examines the rf discharge structure in mixtures of Ar and CF₄ at different ratios, by means of a one-dimensional particle-in-cell/Monte Carlo (PIC/MC) model. A PIC simulation treats the charged particles in a kinetic way. It is attractive because the fields and the energy distributions are obtained self consistently from first principles.²² The collisions between the charged particles are added by combining the PIC model with a MC procedure. The major disadvantage of this method is that it requires a long computational time to reach convergence when the particle density is high (i.e. more “superparticles” have to be followed on a finer grid) or when an electronegative discharge is simulated. In the latter case the negative charges are confined in the bulk plasma and the only loss mechanism, i.e., ion–ion recombination, has a relatively low reaction frequency. Birdsall and co-workers point out many physical and numerical methods of speeding up the PIC calculations.²³ Some of these methods, such as longer ion time steps, different weights for electrons and ions, and improved initial density profiles, are applied in this simulation. In Sec. II the input parameters, the outline of the model, and the collisions included in the simulation are given. In Sec. III the results of the simulation, such as the electric field, the densities, the particle energies, and collision rates are presented and discussed. Finally, in Sec. IV a summary is given.

II. DESCRIPTION OF THE MODEL

The model is developed for a cc rf reactor. It is a cylindrical vacuum chamber containing two planar electrodes separated by a distance $d=2.5$ cm and driven by a rf power source. The amplitude and the frequency of the applied voltage to one of the electrodes are $V=200$ V and $f=13.56$ MHz, respectively. The other electrode is grounded. The gas pressure is fixed at 200 mTorr. It should, however, be mentioned that the model presented here can be applied to other discharge conditions. The computation is based on a one-dimensional coordinate space and three-dimensional velocity space PIC/MC algorithm. The motion of the charged particles is simulated by the PIC method using the standard explicit “leap frog” finite difference scheme. A detailed description of the PIC technique can be found in Birdsall and Langdon.²² Electrons are absorbed and ions are neutralized on the electrodes. Secondary electron emission is not included here because the rf discharge is assumed to be in α regime at the conditions under study (see above).^{24,25} The initial densities of the charged species in the model are based on experimental and simulation data,^{12,16,18} the initial velocities are calculated from the Maxwellian distribution at an average electron temperature of 2 eV and an average ion temperature of 0.043 eV (500 K).²

The charged species taken into account in the model are: electrons, two kinds of positive ions (Ar⁺, CF₃⁺) and two kinds of negative ions (F⁻, CF₃⁻). Simulation results in a

pure cc rf CF₄ discharge show that the dominant positive ions are CF₃⁺, with a density exceeding those of CF₂⁺, CF⁺, C⁺, and F⁺ by more than 2–3 orders of magnitude, and $N_{\text{CF}_3^+} \cong N_{\text{F}^-} + N_{\text{CF}_3^-} + N_e$, where N denotes the number densities in the bulk plasma.¹⁶ For that reason CF₃⁺ is the only type of positive ions of CF₄ followed in the model. It should be mentioned, however, that in a CF₄ inductively coupled plasma (ICP) both measured and calculated data show that the number densities of CF₃⁺, CF₂⁺, CF⁺, and F⁺ are comparable at low pressure and high power in the ICP.^{4,6}

The interactions between the particles are treated by a Monte Carlo method, which is basically a probabilistic approach. To calculate collision probabilities, it is necessary to have the corresponding collision cross-section data, which are not always available. Hence, the present model uses several techniques to define the collision probabilities even when the collision cross sections are unknown (see below).

The electron–neutral collision probability P_{null} is determined by the null collision method for each time step Δt ¹⁸

$$P_{\text{null}} = 1 - \exp[-\nu_c \Delta t], \quad (1)$$

where ν_c is a constant collision frequency, which is obtained once at the beginning of the calculation from¹⁸

$$\nu_c = \max_z(n_g) \max_\varepsilon \left[\left(\frac{2\varepsilon}{m_p} \right)^{1/2} \sum_j \sigma_j(\varepsilon) \right], \quad (2)$$

where n_g is the local density of the neutrals, which is assumed to be constant (i.e., the neutral gas is assumed uniformly distributed in the discharge), m_p is the electron mass, ε is the kinetic energy of each of the electrons, and $\sigma_j(\varepsilon)$ is the cross section of collision type j between the electrons and neutrals. The colliding electrons are chosen randomly and each electron is checked for the type of collision. Vahedi and Surendra¹⁸ describe in detail the null collision technique as well as the method of determining the particle velocities after collision. In the present model, however, the expression for determining the electron scattering angle differs from the one proposed in Ref. 18, as it is explained in Ref. 26.

The electron–neutral collisions considered in this simulation, along with the corresponding threshold energy, and the references for the cross-section data are presented in Table I. Those electron–CF₄ collisions which have small collision cross sections and high threshold energies, such as some ionization reactions,²⁸ are not included in the simulation and are therefore not mentioned in the table either.

The Ar⁺–Ar collision probability is determined by means of the null collision technique. In Eq. (2) m_p , ε , and $\sigma_j(\varepsilon)$, $j=1,2$ now denote the ion mass, the kinetic energy of the argon ion, and the cross sections for elastic isotropic scattering ($j=1$) and for scattering in the backward direction ($j=2$) (to simulate charge transfer), respectively. For more details and for the cross-section data, see Ref. 18.

The CF₃⁺–CF₄, F⁻–CF₄, and CF₃⁻–CF₄ elastic and reactive collisions are simulated using the ion–molecule collision model for endothermic reactions developed by Nanbu and Denpoh (see Refs. 16,30, and 31). The total cross section

TABLE I. Electron-neutral (Ar, CF₄) collisions considered in the model, threshold energy for every reaction, and references for the cross-section data.

Type of collision	Reaction	Threshold (eV)	Ref.
Ar			
Elastic scattering	$e + \text{Ar} \rightarrow e + \text{Ar}$		27
Total electronic excitation	$e + \text{Ar} \rightarrow e + \text{Ar}^*$	12	27
Ionization	$e + \text{Ar} \rightarrow 2e + \text{Ar}^+$	15.7	27
CF ₄			
Momentum transfer	$e + \text{CF}_4 \rightarrow e + \text{CF}_4$		28
Vibrational excitation	$e + \text{CF}_4 \rightarrow e + \text{CF}_4(\nu 1)$	0.108	28
Vibrational excitation	$e + \text{CF}_4 \rightarrow e + \text{CF}_4(\nu 3)$	0.168	28
Vibrational excitation	$e + \text{CF}_4 \rightarrow e + \text{CF}_4(\nu 4)$	0.077	28
Total electronic excitation	$e + \text{CF}_4 \rightarrow e + \text{CF}_4^*$	7.54	28
Electron attachment	$e + \text{CF}_4 \rightarrow \text{F}^- + \text{CF}_3$	6.4	28
Electron attachment	$e + \text{CF}_4 \rightarrow \text{F} + \text{CF}_3^-$	5	29
Dissociation	$e + \text{CF}_4 \rightarrow e + \text{F}^- + \text{CF}_3^+$	12	29
Dissociative ionization	$e + \text{CF}_4 \rightarrow 2e + \text{F} + \text{CF}_3^+$	16	28
Neutral dissociation	$e + \text{CF}_4 \rightarrow e + \text{F} + \text{CF}_3$	12	28
Neutral dissociation	$e + \text{CF}_4 \rightarrow e + 2\text{F} + \text{CF}_2$	17	28
Neutral dissociation	$e + \text{CF}_4 \rightarrow e + 3\text{F} + \text{CF}$	18	28

σ_i of the ion-molecule collisions is derived from the Langevin-Hasse model and in the case of singly charged ions it is given by³¹

$$\sigma_i = \left(\frac{\pi \alpha_p e^2}{\epsilon_0 \mu} \right)^{1/2} \beta_\infty^2 g^{-1}, \quad (3)$$

where μ is the reduced mass, e is the electron charge, ϵ_0 is the dielectric constant of vacuum, α_p is the polarizability, $g = |V_i - V_n|$ is the relative velocity, V_i and V_n being the precollision velocities of the ion and neutral particle respectively, and β_∞ is the value of the dimensionless impact parameter β , for which the deflection angle is negligibly small. The value of β_∞ is set to 3 for both Ar and CF₄.^{30,31} For Ar and CF₄ the polarizability α_p is equal to $11.08a_0^3$ and $19.0a_0^3$, respectively, where a_0 is the Bohr radius.¹

Hence the ion-molecule collision probability, $P_c = n_g g \sigma_i \Delta t$ for the time step Δt at a neutral gas density n_g equals

$$P_c = \left(\frac{\pi \alpha_p e^2}{\epsilon_0 \mu} \right)^{1/2} \beta_\infty^2 n_g \Delta t. \quad (4)$$

For every colliding ion, the value of the dimensionless impact parameter β is determined by a random number R , i.e. $\beta = \beta_\infty(R)^{1/2}$.³⁰ The critical value of β for reactive collisions is equal to one, i.e. for $\beta \leq 1$ a reactive collision occurs.¹⁶ It should be mentioned that a reactive collision is specified as an elastic collision with isotropic scattering whenever the colliding pair of an ion and a molecule are unchanged after the collision. For simplicity, this is called as “elastic reactive” collision further in the text. For $\beta > 1$, on the other hand, the collision is assumed to be elastic with anisotropic scattering. A description of how to determine the ion velocity after elastic collision with anisotropic scattering is given in Ref. 31.

In a reactive collision, the colliding ion and molecule, called reactants, form a complex, which separates to products via the i th reaction path. As mentioned above, when the

TABLE II. CF₃⁺-CF₄ reactions considered in the model and the corresponding thermodynamic threshold energies ΔE , adopted from Refs. 16 and 30.

CF ₃ ⁺ +CF ₄ →	ΔE (eV)	CF ₃ ⁺ +CF ₄ →	ΔE (eV)
1. CF ₃ ⁺ +CF ₃ +F	5.621	21. CF ₂ ⁺ +CF+F ₂ +2F	19.024
2. CF ₂ ⁺ +CF ₄ +F	5.843	22. CF ₃ ⁺ +C+4F	20.392
3. CF ₂ ⁺ +CF ₄ +F ₂	7.546	23. CF ₂ ⁺ +CF+4F	20.624
4. CF ₃ ⁺ +CF ₂ +F ₂	7.598	24. CF ⁺ +CF+2F ₂ +F	20.727
5. CF ⁺ +CF ₄ +2F	9.146	25. CF ⁺ +CF+F ₂ +3F	22.327
6. CF ₃ ⁺ +CF ₂ +2F	9.198	26. CF ₂ ⁺ +C+2F ₂ +F	23.035
7. CF ₂ ⁺ +CF ₃ +F ₂	9.864	27. CF ⁺ +CF+5F	23.927
8. CF ₂ ⁺ +CF ₃ +2F	11.464	28. CF ₂ ⁺ +C+F ₂ +3F	24.635
9. CF ⁺ +CF ₃ +F ₂ +F	13.167	29. CF ⁺ +C+3F ₂	24.738
10. CF ₃ ⁺ +CF+F ₂ +F	13.181	30. CF ₂ ⁺ +C+5F	26.235
11. CF ₂ ⁺ +CF ₂ +F ₂ +F	13.441	31. CF ⁺ +C+2F ₂ +2F	26.338
12. CF ⁺ +CF ₃ +3F	14.767	32. CF ⁺ +C+F ₂ +4F	27.938
13. CF ₃ ⁺ +CF+3F	14.781	33. CF ⁺ +C+6F	29.538
14. CF ₂ ⁺ +CF ₂ +3F	15.041	34. C ⁺ +C+3F ₂ +F	32.555
15. CF ⁺ +CF ₂ +2F ₂	15.144	35. C ⁺ +C+2F ₂ +3F	34.155
16. CF ⁺ +CF ₂ +F ₂ +2F	16.744	36. C ⁺ +C+F ₂ +5F	35.755
17. CF ₃ ⁺ +C+2F ₂	17.192	37. C ⁺ +C+7F	37.355
18. CF ₂ ⁺ +CF+2F ₂	17.424	38. F ⁺ +2C+3F ₂	38.717
19. CF ⁺ +CF ₂ +4F	18.344	39. F ⁺ +2C+2F ₂ +2F	40.317
20. CF ₃ ⁺ +C+F ₂ +2F	18.792	40. F ⁺ +2C+F ₂ +4F	41.917
		41. F ⁺ +2C+6F	43.517

products are the same as the colliding particles, the collision is specified as “elastic reactive.” The reaction rate of the i th reaction and the rate of the “elastic reactive” collision are determined by applying the Rice-Rampersperger-Kassel theory.¹⁶ Hence the probability P_{r-i} of generating products from the complex via the i th reaction path is given by¹⁶

$$P_{r-i} = \frac{(\epsilon - \Delta E_i)^{s-1}}{I + \sum_{i=1}^I (\epsilon - \Delta E_i)^{s-1}}, \quad (5)$$

where $\epsilon = \mu g^2/2$ is the relative kinetic energy of the reactants, ΔE_i is the thermodynamic threshold energy of the i th reaction, s is the number of vibrational modes of the complex, and I is the number of reaction paths satisfying $\epsilon > \Delta E_i$. The number of vibrational modes is described as $s = (3N - 6)/2$, where N is the number of atoms forming the complex.¹⁶

Similarly, the probability of “elastic reactive” collision P_{el} is expressed by¹⁶

$$P_{el} = \frac{\epsilon^{s-1}}{I + \sum_{i=1}^I (\epsilon - \Delta E_i)^{s-1}}. \quad (6)$$

According to the probabilities P_{r-i} and P_{el} a reaction path is randomly sampled from 1 to $(I+1)$, where $(I+1)$ denotes the “elastic reactive” collision.¹⁶

All reactions of CF₃⁺, F⁻, or CF₃⁻ with CF₄ considered in the model and the corresponding thermodynamic threshold energies ΔE are given in Tables II, III, and IV, respectively. All data for the reactions, the method of sampling the reaction path according to the probabilities P_{r-i} and P_{el} , and the method of calculating the product velocities are adopted from Refs. 16 and 30.

TABLE III. $F^- - CF_4$ reactions considered in the model and the corresponding thermodynamic threshold energies ΔE , adopted from Refs. 16 and 30.

$F^- + CF_4 \rightarrow$	ΔE (eV)	$F^- + CF_4 \rightarrow$	ΔE (eV)
1. $CF_4 + F + e$	3.521	11. $CF + 2F_2 + e$	15.102
2. $F^- + CF_3 + F$	5.621	12. $CF + F_2 + 2F + e$	16.702
3. $CF_3 + F_2 + e$	7.542	13. $F^- + C + 2F_2$	17.192
4. $F^- + CF_2 + F_2$	7.598	14. $CF + 4F + e$	18.302
5. $CF_3 + 2F + e$	9.142	15. $F^- + C + F_2 + 2F$	18.792
6. $F^- + CF_2 + 2F$	9.198	16. $F^- + C + 4F$	20.392
7. $CF_2 + F_2 + F + e$	11.119	17. $C + 2F_2 + F + e$	20.713
8. $CF_2 + 3F + e$	12.719	18. $C + F_2 + 3F + e$	22.313
9. $F^- + CF + F_2 + F$	13.181	19. $C + 5F + e$	23.913
10. $F^- + CF + 3F$	14.781		

In the simulation the $Ar^+ - CF_4$, $CF_3^+ - Ar$, $F^- - Ar$, and $CF_3^- - Ar$ elastic collisions are treated by means of the same technique. Anisotropic scattering is assumed for $\beta > 1$ and isotropic scattering for $\beta \leq 1$.

Cross-section data for positive-negative ion recombination are hard to find in the literature. In the model the recombination cross section and hence the probability is determined from a given expression for the corresponding rate constant, as proposed by Nanbu and Denpoh.³² If the num-

TABLE IV. $CF_3^- - CF_4$ reactions considered in the model and the corresponding thermodynamic threshold energies ΔE , adopted from Refs. 16 and 30.

$CF_3^- + CF_4 \rightarrow$	ΔE (eV)	$CF_3^- + CF_4 \rightarrow$	ΔE (eV)
1. $CF_3 + CF_4 + e$	1.871	35. $CF_3^- + C + F_2 + 2F$	18.792
2. $F^- + CF_2 + CF_4$	1.927	36. $CF_3 + C + 2F_2 + e$	19.063
3. $CF_2 + CF_4 + F + e$	5.448	37. $F^- + 2CF + 2F_2$	19.091
4. $CF_3^- + CF_3 + F$	5.621	38. $F^- + CF_2 + C + 2F_2$	19.119
5. $2CF_3 + F + e$	7.492	39. $CF_2 + CF + 4F + e$	20.229
6. $F^- + CF + CF_4 + F$	7.510	40. $CF_3^- + C + 4F$	20.392
7. $F^- + CF_2 + CF_3 + F$	7.548	41. $CF_3 + C + F_2 + 2F + e$	20.663
8. $CF_3^- + CF_2 + F_2$	7.598	42. $F^- + 2CF + F_2 + 2F$	20.691
9. $CF_3^- + CF_2 + 2F$	9.198	43. $F^- + CF_2 + C + F_2 + 2F$	20.719
10. $CF + CF_4 + F_2 + e$	9.431	44. $CF_3 + C + 4F + e$	22.263
11. $CF_3 + CF_2 + F_2 + e$	9.469	45. $F^- + 2CF + 4F$	22.291
12. $F^- + 2CF_2 + F_2$	9.525	46. $F^- + CF_2 + C + 4F$	22.319
13. $CF + CF_4 + 2F + e$	11.031	47. $2CF + 2F_2 + F + e$	22.612
14. $CF_3 + CF_2 + 2F + e$	11.069	48. $CF_2 + C + 2F_2 + F + e$	22.640
15. $F^- + 2CF_2 + 2F$	11.125	49. $2CF + F_2 + 3F + e$	24.212
16. $F^- + CF + CF_3 + F_2$	11.531	50. $CF_2 + C + F_2 + 3F + e$	24.240
17. $2CF_2 + F_2 + F + e$	13.046	51. $F^- + CF + C + 2F_2 + F$	24.702
18. $F^- + CF + CF_3 + 2F$	13.131	52. $2CF + 5F + e$	25.812
19. $CF_3^- + CF + F_2 + F$	13.181	53. $CF_2 + C + 5F + e$	25.840
20. $F^- + C + CF_4 + F_2$	14.219	54. $F^- + CF + C + F_2 + 3F$	26.302
21. $2CF_2 + 3F + e$	14.646	55. $CF + C + 3F_2 + e$	26.623
22. $CF_3^- + CF + 3F$	14.781	56. $F^- + CF + C + 5F$	27.902
23. $C + CF_4 + F_2 + F + e$	15.042	57. $CF + C + 2F_2 + 2F + e$	28.223
24. $CF_3 + CF + F_2 + F + e$	15.052	58. $F^- + 2C + 3F_2$	28.713
25. $F^- + CF_2 + CF + F_2 + F$	15.108	59. $CF + C + F_2 + 4F + e$	29.823
26. $F^- + C + CF_4 + 2F$	15.819	60. $F^- + 2C + 2F_2 + 2F$	30.313
27. $C + CF_4 + 3F + e$	16.642	61. $CF + C + 6F + e$	31.423
28. $CF_3 + CF + 3F + e$	16.652	62. $F^- + 2C + F_2 + 4F$	31.913
29. $F^- + CF_2 + CF + 3F$	16.708	63. $2C + 3F_2 + F + e$	32.234
30. $CF_2 + CF + 2F_2 + e$	17.029	64. $F^- + 2C + 6F$	33.513
31. $F^- + C + CF_3 + F_2 + F$	17.142	65. $2C + 2F_2 + 3F + e$	33.834
32. $CF_3^- + C + 2F_2$	17.192	66. $2C + F_2 + 5F + e$	35.434
33. $CF_2 + CF + F_2 + 2F + e$	18.629	67. $2C + 7F + e$	37.034
34. $F^- + C + CF_3 + 3F$	18.742		

TABLE V. Positive-negative ion recombination reactions considered in the model and the corresponding recombination rate coefficients, adopted from Ref. 10.

Reaction	Rate coefficient ($m^3 s^{-1}$)
$F^- + Ar^+ \rightarrow F + Ar$	1.0×10^{-13}
$F^- + CF_3^+ \rightarrow F + CF_3$	1.0×10^{-13}
$CF_3^- + Ar^+ \rightarrow CF_3 + Ar$	1.0×10^{-13}
$CF_3^- + CF_3^+ \rightarrow CF_3 + CF_3$	1.0×10^{-13}

bers of the simulated positive (A^+) and negative ions (B^-) in a cell with volume V_c are N_A and N_B , respectively, and if the weight of the superparticles (representing the real particles) is W , then the number of recombination pairs N_r in a time Δt_r in a cell is³²

$$N_r = W \frac{N_A N_B}{V_c} k_0 \Delta t_r, \quad (7)$$

where k_0 is the rate constant at temperature T_0 [i.e., the reaction rate constant is a function of temperature T : $k_r(T) = k_0(T_0/T)^n$, $n \geq 0$]. Note that N_r is the number of superparticles that recombines. When the weight W is different for the different kinds of ions, as in the present simulation, a revision of Eq. (7) is required and $N_{rA} W_A$ has to be equal to $N_{rB} W_B$, where N_{rA} and N_{rB} are the recombination numbers of superparticles of types A and B, respectively. The positive-negative ion recombinations and the corresponding rate constants are presented in Table V. The data are taken from Rauf and Kushner.¹⁰ In the simulation the recombination time step Δt_r is taken to be 10^5 times longer than the electron time step; the probability for recombination is, indeed, low because of the much lower ion densities in comparison with the neutral gas density.

III. RESULTS AND DISCUSSION

The calculations are performed in one dimension for Ar/ CF_4 mixtures at molar ratios of 0.1/0.9, 0.5/0.5 and 0.9/0.1, and for pure Ar and pure CF_4 discharges. In Figs. 1–7 the axis at $z=0$ is the rf powered electrode and the one at $z=2.5$ cm is the grounded electrode. The gas temperature is set to 300 K. The simulation grid is uniform and it consists of 100 cells. The electron time step is 3.7×10^{-11} s for an Ar discharge simulation and 7.4×10^{-11} s for all other simulations. To speed up the calculation, the ion time step is set to be 25 times longer than the electron time step. The choice of the grid spacing and the time steps is defined by the accuracy criteria for PIC/MC codes with explicit mover.²³ Typical results of this model are electron and ion densities, fluxes and energy distributions, collision rates, and electric field and potential distributions.

A. Pure Ar discharge

Figure 1 presents the simulation results of the electric field distribution at four phases (a), the charged particle density distributions (b), the average electron and argon-ion energies (c), and the time-averaged ionization rate (d) in a pure Ar discharge. In the bulk plasma the potential is nearly constant and therefore the electric field is weak. Strong electric

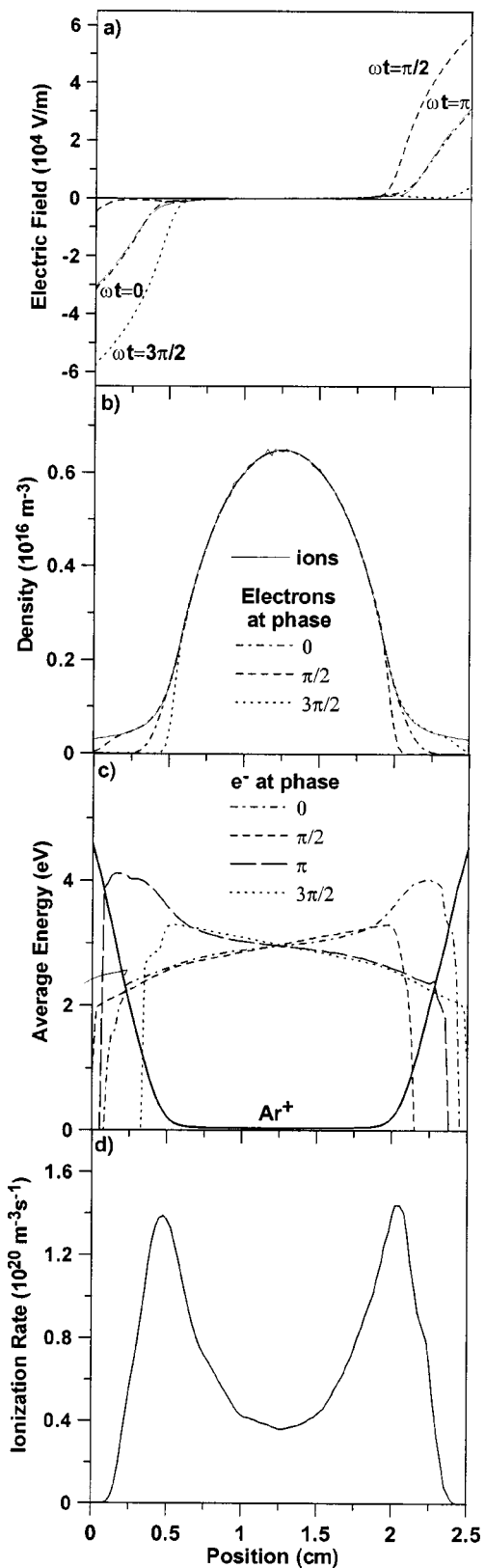


FIG. 1. Electric field distribution at four phases (a), electron and Ar⁺ ion density distributions (b), average electron and Ar⁺ ion energies (c), and time-averaged ionization rate (d) in a pure Ar discharge at $p=200$ mTorr and $\gamma=0$.

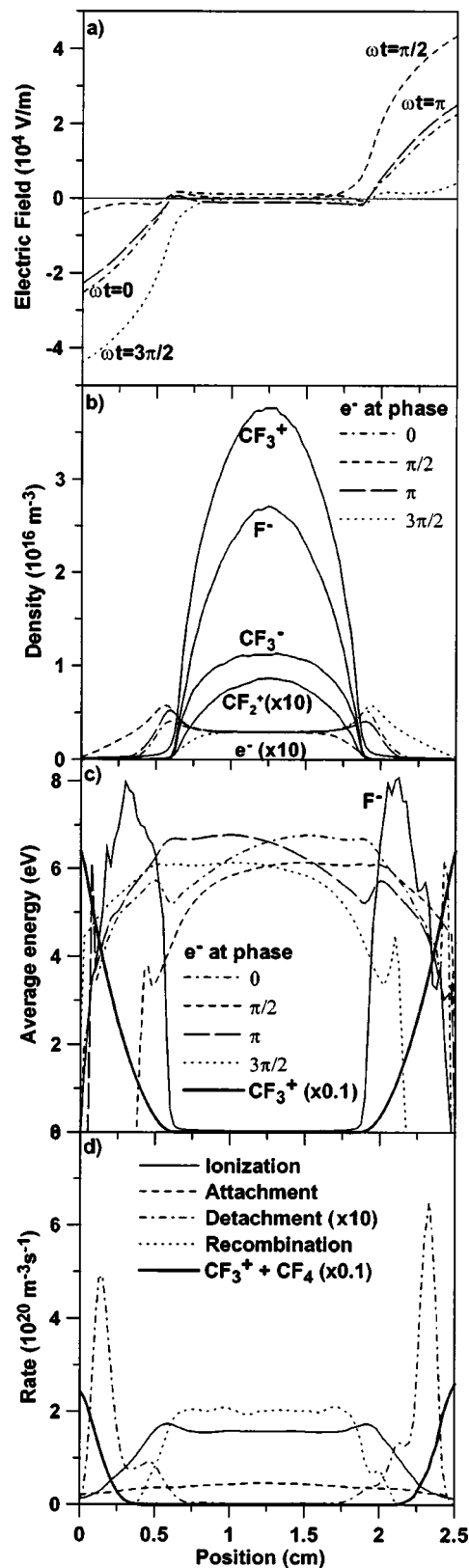


FIG. 2. Electric field distribution at four phases (a), charged particle density distributions (b), average electron and ion energies (c) and the time-averaged reaction rates (d) in a pure CF₄ discharge at $p=200$ mTorr and $\gamma=0$.

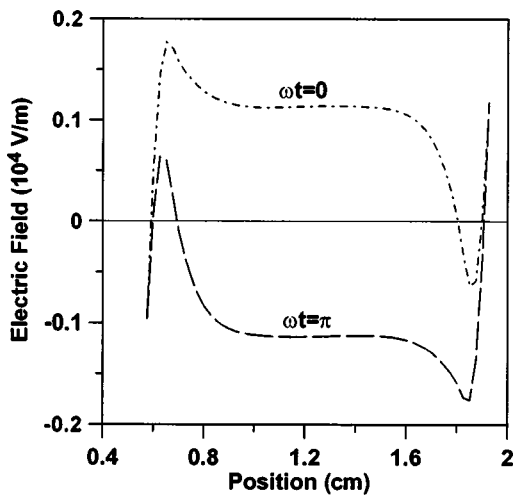


FIG. 3. Electric field distribution at phases 0 and π in the bulk plasma in a pure CF_4 discharge at $p=200$ mTorr and $\gamma=0$.

fields are found in the sheath regions, where the voltage drops are concentrated. The only charged particles are Ar^+ ions and electrons [Fig. 1(b)]. As expected, the ion density profile is constant throughout the rf cycle, since the ions cannot follow the rapidly fluctuating electric field, whereas the electron density profile varies largely in the sheaths. At $\omega t = \pi/2$ the electron density in the left sheath is approximately equal to the Ar^+ density and has a more or less constant value. However, the electron density in the right sheath decreases rapidly to zero toward the grounded electrode at this time in the rf cycle. As the cycle advances, the electrons move to the right sheath and the density profile at $\omega t = 3\pi/2$ is a mirror image of that at phase $\pi/2$. At phases 0 and π the electron density decreases to zero toward both electrodes but less rapidly than at phases $3\pi/2$ and $\pi/2$, respectively. The electron density profile at $\omega t = \pi$ is not shown in the picture because it is very similar to the profile at $\omega t = 0$. The movement of the electrons causes the modulation of the sheath width.

The average electron energy is around 3 eV in the bulk plasma [see Fig. 1(c)] and it reaches its maximum of 4 eV in the sheath. To investigate the role of the secondary electron emission on the discharge properties the simulation was carried out with a secondary electron emission coefficient of 0.03. The results are not presented in the article since they confirm that the discharge is indeed in the α regime. In this regime the effect of secondary electron emission on most plasma parameters is rather small except for the average electron energy in the sheath where high electron energy peaks are observed, in agreement with previous investigations of an Ar discharge (cf. Ref. 17). The Ar^+ ion energy is around 0.04 eV in the bulk plasma. The argon ions are accelerated toward the electrodes in the sheath and therefore the ions have their maximum energy close to the electrodes, which is about 4.5 eV in this simulation.

The time-averaged ionization rate has maxima at the bulk-sheath interface [Fig. 1(d)]. The simulation results for the ionization rate at different phases of the rf cycle, which are not presented here, show that the right peak appears at

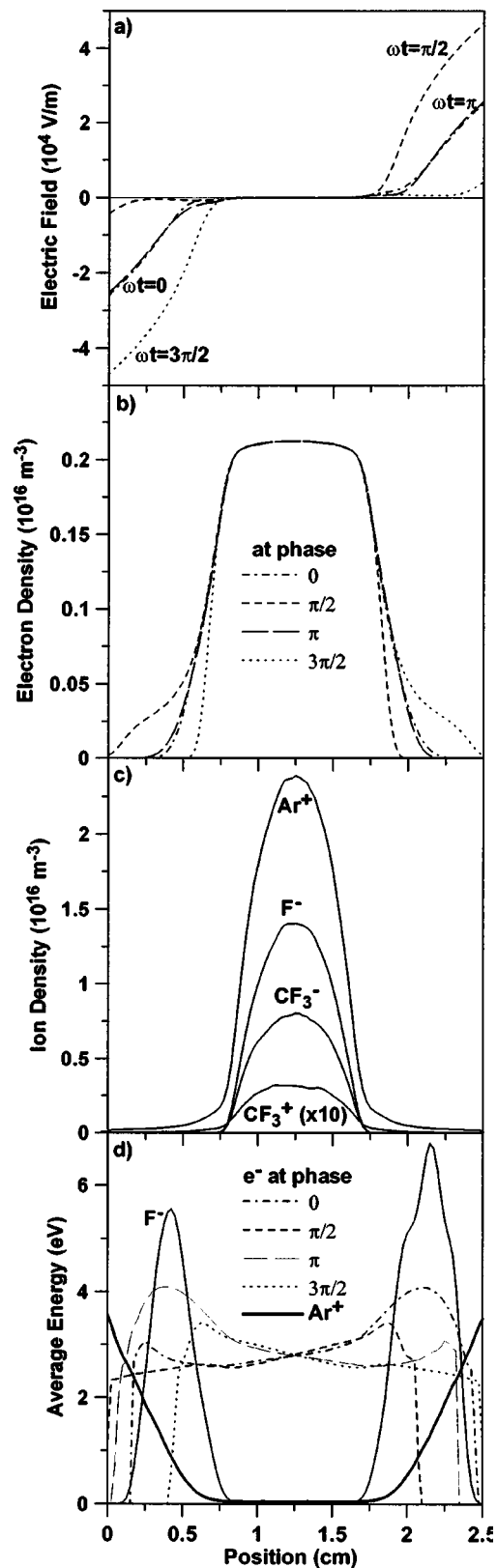


FIG. 4. Electric field (a) and electron density (b) at four times in the rf cycle, ion densities (c), and average electron, Ar^+ and F^- ion energies (d) in an Ar/CF_4 (0.9/0.1) discharge at $p=200$ mTorr and $\gamma=0$.

phase 0 and the left one at phase π , i.e., the maxima of the ionization collisions do not coincide with the nonzero values of the electron density in the sheaths (see above). The ionization peaks appear because of the energy gained by the

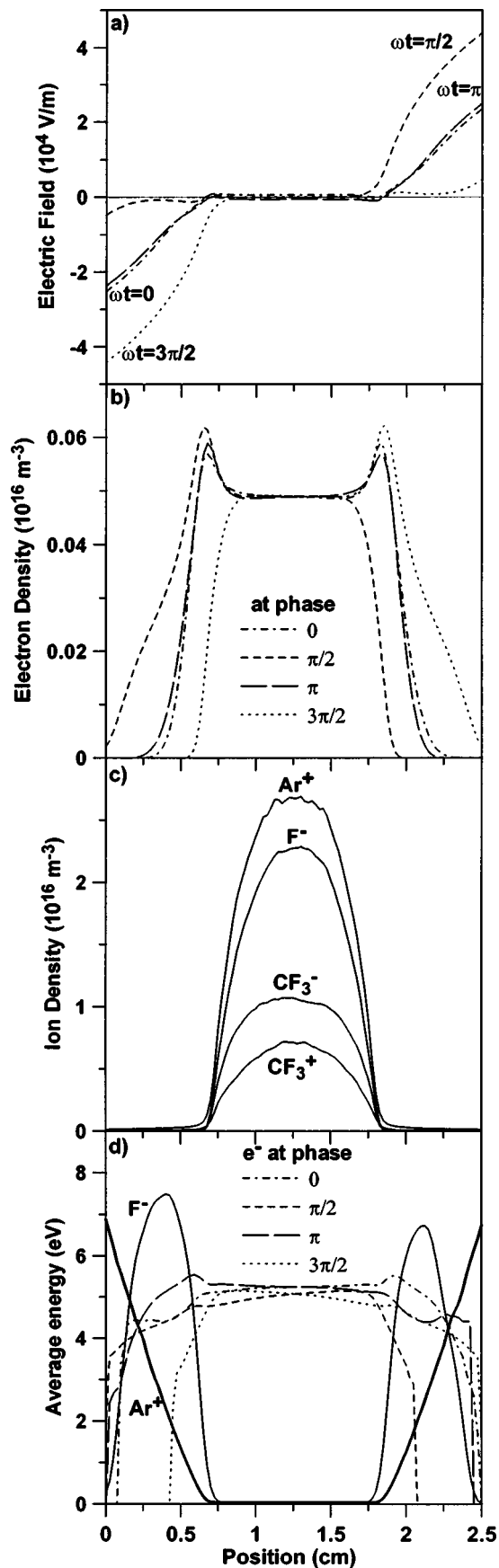


FIG. 5. Electric field (a) and electron density (b) at four times in the rf cycle, ion densities (c), and average electron, Ar^+ and F^- ion energies (d) in an Ar/CF_4 (0.5/0.5) discharge at $p=200$ mTorr and $\gamma=0$.

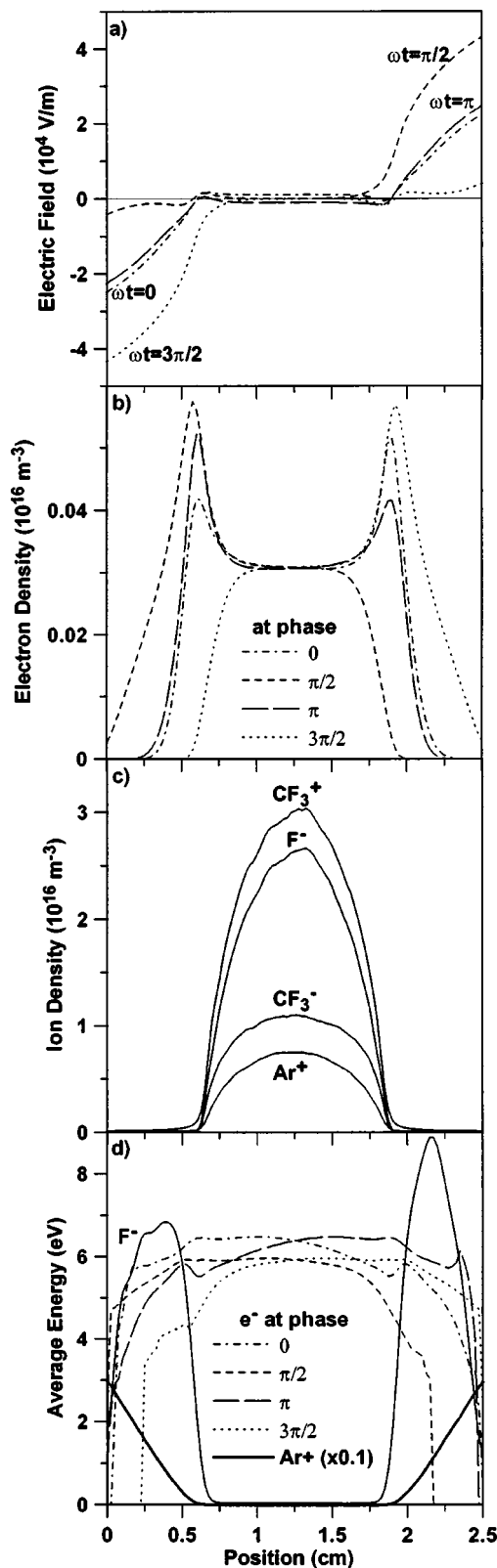


FIG. 6. Electric field (a) and electron density (b) at four times in the rf cycle, ion densities (c), and average electron, Ar^+ and F^- ion energies (d) in an Ar/CF_4 (0.1/0.9) discharge at $p=200$ mTorr and $\gamma=0$.

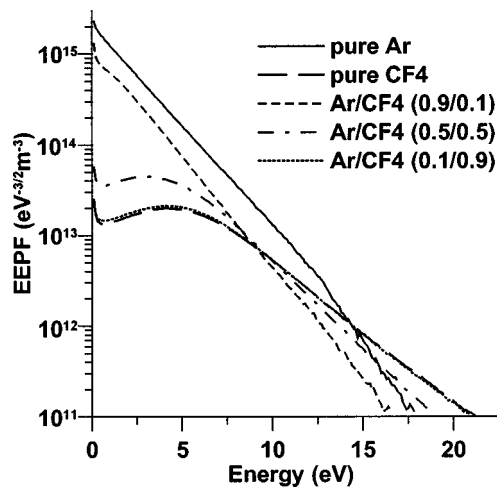


FIG. 7. The EPPF for five simulated gas mixtures at $p=200$ mTorr and $\gamma=0$.

electrons during their acceleration away from the electrodes into the discharge [cf. the maximum values of the electron energy at phase 0 and π in Fig. 1(c)].

All the characteristic features of the Ar discharge discussed here are in agreement with those available in the literature (e.g., see Refs. 1 and 17–20).

B. Pure CF_4 discharge

The electric field distribution at four phases (a), the charged particle density distributions (b), the average electron and ion energies (c), and the time-averaged reaction rates (d) in a pure CF_4 discharge are shown in Fig. 2. The structure of the discharge is typically electronegative and is characterized by the presence of negative ions (F^- and CF_3^-), which are the dominant negative charged species. Indeed, the electron density in the bulk is about 50 times less than the density of the major negative ion F^- [see Fig. 2(b)]. Unlike in the Ar discharge the electric field in the bulk plasma is substantial (on the order of 1000 V/m) [Figs. 2(a) and Fig. 3] since the potential is not constant. Another difference with the electropositive discharge is the appearance of the double layer structure (i.e., the local maxima or minima of the electric field) near the bulk–sheath interface, which is related to the density distribution. Moreover, a field reversal is observed at the right bulk–sheath interface at phase 0 and at the left bulk–sheath interface at phase π , respectively (see Fig. 3). The ion density profiles [Fig. 2(b)] are constant in time throughout the rf cycle, like in the Ar discharge. Since the diffusive flux of the negative ions is very low and the electric field is always directed outward, the negative ions are confined in the bulk plasma and are almost absent in the sheath. In the sheath mainly positive ions and electrons are found. The electrons move toward one of the electrodes depending on the phase of the applied potential. Their movement affects the local fields, which are developed by the differences of positive and negative ion concentration near the electrodes, and they cause the electrons to pile up in

the bulk–sheath region. Hence, peaks in the electron density appear at the bulk–sheath interface, which cannot be observed in electropositive discharges.

Because of the nonzero bulk electric field the average electron energy in the bulk plasma is higher than in a pure Ar discharge and its value is around 6 eV [Fig. 2(c)]. Like in the Ar discharge high electron energy peaks are not observed in the sheath since the secondary electron emission coefficient is set to 0 (contrary to Ref. 16, where gamma has a nonzero value). All ions have constant average energy around 0.04 eV in the bulk plasma, i.e., the ion temperature is close to the gas temperature, because of the frequent collisions with the neutral molecules.¹ The positive CF_3^+ ions gain energy in the sheath like the argon ions and their energy at the electrodes has a maximum value of around 65 eV [Fig. 2(c)]. As described above, few negative ions exist in the sheath. Negative ions are produced by electron attachment; the attachment rate is shown in Fig. 2(d). They are accelerated toward the bulk plasma and then are pushed back by the double layer. Therefore the negative ions gain energy in the sheath by oscillating between the electrodes and the bulk–sheath interface, and their average energy reaches a maximum of 8 eV [see Fig. 2(c)]. The average energy of the CF_3^- ions is not given because its profile and value are similar to that of the F^- ions.

Time-averaged rates for ionization, electron attachment, electron detachment, positive–negative ion recombination, and $\text{CF}_3^+ - \text{CF}_4$ reactive collisions are shown in Fig. 2(d). The electron attachment, electron detachment, and ion–ion recombination are represented as the sum of all corresponding reaction collisions. Ionization and electron attachment occur anywhere in the discharge space. The electron attachment rate is lower than the ionization rate because of the smaller cross section. The electron detachment occurs in the sheath where the negative ion energy is high enough (see the threshold energies for the detachment processes in Tables III and IV). Similarly, the $\text{CF}_3^+ - \text{CF}_4$ reaction rate, which is again taken as the sum of all reactions, shows that the reactive collisions take place in the sheath. The positive–negative ion recombination is observed only in the bulk plasma and is the major loss process of negative ions.

The simulation results for the electric field, the particle densities and energies, and collision rates are in reasonable agreement with the simulation results of Denpoh and Nanbu¹⁶ except for the ion density profiles in the bulk plasma, which are parabolic in the present calculation. Concave ion density profiles are observed in other simulations of a CF_4 discharge^{14,15} as well as in other electronegative discharges¹⁴ when ionization exceeds ion–ion recombination in the plasma–sheath interface. A possible explanation for the present results is that this simulation does not follow all CF_4 positive ions because of their much lower density compared to the CF_3^+ density (see Sec. II). This simplification is done because the aim of the present model is actually to study the discharge properties in Ar/ CF_4 mixtures. Moreover, the concentration of CF_4 does not exceed 10% for etching purposes in practice, which suggests that the effect of all CF_4 ions, except for CF_3^+ , on the plasma parameters will be negligible in such mixtures (see the results below).

C. Ar/CF₄ mixtures

Figures 4, 5, and 6 show the structure of the discharge in an Ar/CF₄ mixture for a ratio of 0.9/0.1, 0.5/0.5, and 0.1/0.9, respectively. The electric field (a) and electron density (b) at four times in the rf cycle, the time-averaged ion densities (c), and the average electron (at four phases), Ar⁺ and F⁻ ion energies (d) are presented for each of the three gas compositions. The average energy of the CF₃⁺ ions is not presented since it has a similar profile and value as in a pure CF₄ discharge [see Fig. 2(c)]. The average energy of the CF₃⁻ ions is not given either, because its profile and value are similar to that of the F⁻ ions. Based on the results for pure Ar and CF₄ discharges, described above, a comparative analysis of the discharge structure in a mixture of Ar and CF₄ is carried out here.

At high concentration of Ar (90%) the structure of the discharge is similar to that of an electropositive discharge (Fig. 4). The electric field distribution resembles that of a pure Ar discharge [cf. Figs. 1(a) and 4(a)]. The major positive ions are Ar⁺ ions; the density of CF₃⁺ in the center of the bulk plasma is about 2 orders of magnitude lower than that of Ar⁺ [Fig. 4(c)]. Similar ion composition was measured in an Ar/CF₄ ICP,^{3,5} although quantitative comparison is difficult to make because of the differences in the operating conditions of capacitively and inductively coupled discharges.

Some features of electronegative discharges begin to appear in Fig. 4. The dominant negative carriers are not the electrons, but the negative ions (F⁻ and to a lesser extent CF₃⁻). In the bulk center the F⁻ ion density has a value of $1.4 \times 10^{16} \text{ m}^{-3}$, whereas the electron density is only $2.1 \times 10^{15} \text{ m}^{-3}$ [cf. Figs. 4(b) and 4(c)]. The rapid decrease in the electron density with the addition of even a small amount of CF₄ was also observed in an Ar/CF₄ ICP.³ The electron density profile is quite flat in the bulk plasma and it resembles that of a pure CF₄ discharge, but the peaks at the bulk-sheath interface are not yet formed. Experimental results¹¹ also revealed a flat electron density profile in the bulk plasma at CF₄ concentrations up to 10%.

The average electron energy is around 3 eV in the bulk plasma [Fig. 4(d)] and its profile is similar to the one of a pure Ar discharge. The Ar⁺ ions have a maximum energy of about 3.5 eV at the electrodes. The F⁻ ions reach a maximum energy of 7 eV in the sheath. From the calculated reaction rates (not shown here) it is clear that the ion-CF₄ reactive collisions play no significant role in sustaining the discharge, because of the low concentration of CF₄ molecules.

At equal concentrations of Ar and CF₄ gas (Fig. 5) the discharge exhibits more electronegative features. The double layer structure in the electric field and the maxima in the electron density appear [Figs. 5(a) and 5(b)], as well as the electric field reversal at phases 0 and π . The electron density is about $5 \times 10^{14} \text{ m}^{-3}$ in the bulk, i.e., four times lower than for the 0.9/0.1 gas mixture. At the same time, the F⁻ ion density increases up to $2.4 \times 10^{16} \text{ m}^{-3}$ in the bulk. Similarly, the CF₃⁻ ion density is higher compared to the 0.9/0.1 gas mixture. The Ar⁺ ion is still the major positive ion [Fig. 5(c)] because of the larger ionization cross section of argon

compared to that of CF₄. However, the density of the CF₃⁺ ions is now only less than a factor of 4 lower than the Ar⁺ ion density. Its value in the center is $7 \times 10^{15} \text{ m}^{-3}$ [compared to only $3 \times 10^{14} \text{ m}^{-3}$ at the 0.9/0.1 gas mixture in Fig. 4(c)], as is qualitatively expected because of the higher concentration of CF₄ molecules. The average electron energy is almost constant in the bulk plasma at around 5 eV [Fig. 5(d)]. The Ar⁺ ions have an average energy of 0.04 eV in the bulk plasma, and they reach a maximum average energy of 7 eV at the electrodes, which is two times higher than in the 0.9/0.1 Ar/CF₄ discharge. The average F⁻ ion energy is about 0.035 eV in the bulk plasma and it has a maximum value of 7 eV in the sheath.

At high concentration of CF₄ (90%) the discharge structure is definitely electronegative (Fig. 6). The double layer and the electron density maxima are well established [Figs. 6(a) and 6(b)]. A field reversal is observed at phases 0 and π . The major positive ion is now CF₃⁺ [Fig. 6(c)]. Indeed, the CF₃⁺ density in the bulk plasma has a value of $3 \times 10^{16} \text{ m}^{-3}$, whereas the Ar⁺ density is only $7 \times 10^{15} \text{ m}^{-3}$. Similar dependence of the number densities of the positive ions with the CF₄ content was measured in an inductively coupled Ar/CF₄ discharge.⁵ The F⁻ has a similar, but somewhat lower density than the CF₃⁺ and the CF₃⁻ has a similar, but somewhat higher density than the Ar⁺. The electron density is $3 \times 10^{14} \text{ m}^{-3}$ in the bulk plasma and reaches a maxima of $6 \times 10^{14} \text{ m}^{-3}$ at the bulk-sheath interface. The average electron energy in the bulk is about 6 eV like in a pure CF₄ discharge [cf. Figs. 2(c) and 6(d)]. The maximum value of the average Ar⁺ ion energy is 32 eV. The increase of the Ar⁺ ion energy in the sheath with decreasing Ar concentration shows that the Ar⁺-Ar collisions are the main energy loss term for the Ar⁺ ions. The average F⁻ ion energy again reaches its maximum in the sheath with a value of around 8 eV.

The electron energy probability function (EEPF) $f_e(\varepsilon) (= F_e(\varepsilon)\varepsilon^{-1/2})$ at the center of the discharge is shown in Fig. 7 for all simulated gas mixtures. The calculated EEPF in a pure Ar discharge confirms the previous simulated and measured results.^{21,33} The EEPF in a mixture of Ar and CF₄ changes its profile from Maxwellian like to Druyvesteyn like with the transition from electropositive to electronegative behavior of the discharge. The high-energy tail in the latter case is due to the strong electric field in the bulk (up to 1000 V/m) (see Fig. 3) in comparison with the weak electric field (up to 10V/m) in electropositive discharges. The explanation of the difference in the EEDF $F_e(\varepsilon)$ in electropositive and electronegative discharges can be found in Ref. 21. The calculated EEPF in a pure CF₄ discharge is in good agreement with that presented by Denpoh and Nanbu in Ref. 34 at the same operating conditions.

Finally, to compare the simulation results with the experimental data the developed model is carried out at operating conditions close to those presented in Ref. 11, i.e., for a distance between the electrodes of 6 cm, a pressure ranging from 30 to 100 mTorr and at CF₄ contents from 2% to 10%. The applied voltage amplitude is 240 V. The calculated and measured results for the electronegativity $\alpha_0 (= n_n/n_e)$, where n_n and n_e denote the negative ion and electron densi-

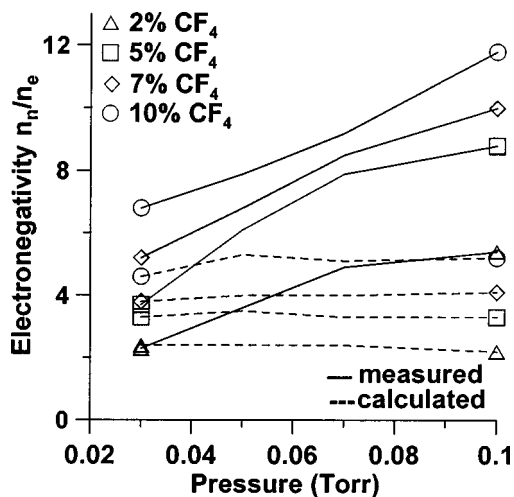


FIG. 8. The measured (solid lines) and calculated (broken lines) electronegativities $\alpha = n_n/n_e$ in an Ar/CF₄ discharge at a concentration of CF₄ up to 10% over the pressure range from 30 to 100 mTorr.

ties, respectively) are presented in Fig. 8. Both measured and calculated electronegativities increase with the CF₄ content. This behavior is as expected since the attachment probability becomes higher with the CF₄ content. However, the simulations cannot yet predict the increase of the measured electronegativity with pressure. Indeed, the probabilities of all kinds of electron-neutral collisions are proportional to the neutral gas density and consequently to the pressure. As a result the densities of all charged particles rise. Therefore the probabilities of all production and loss processes in the model increase with pressure but the ratios of negative ions to electrons stay more or less constant at least in the investigated pressure range.

IV. SUMMARY

A one-dimensional PIC/MC model has been developed to describe the structure of a cc rf discharge in a gas mixture of Ar and CF₄. The model follows five charged particles: electrons, Ar⁺, CF₃⁺, F⁻, and CF₃⁻. The collisions treated by the Monte Carlo method include electron-Ar collisions, electron-CF₄ collisions, various kinds of collisions of CF₃⁺, F⁻, CF₃⁻, or Ar⁺ with Ar or CF₄, and positive-negative ion recombination. The electron-neutral collision probability is determined by the null collision method based on cross-section data for electron-Ar and electron-CF₄ collisions. The Ar⁺-Ar collision probability is calculated in the same way. Since not all collision cross-section data are available, the present model uses several techniques to define the collision probabilities even when the cross sections are unknown. The probability for the positive-negative ion recombination is determined from the recombination rate constant, whereas the ion-neutral elastic and reactive collisions are simulated by an ion-molecule collision model for endothermic reactions.

The simulations are performed for 0.1/0.9, 0.5/0.5, and 0.9/0.1 ratios of Ar/CF₄ mixture, and for pure Ar and pure CF₄ discharge. All calculations are carried out at the following operating conditions: a distance between the electrodes

of 2.5 cm, $V=200$ V, and $f=13.56$ MHz, $p=200$ mTorr, and $\gamma=0$. This model yields results for the electron and various ion densities, their fluxes and energy distributions, the collision rates, and the electric field and potential distributions.

First of all, the structures of the pure electropositive Ar discharge and of the pure electronegative CF₄ discharge are clarified. Then the results for Ar/CF₄ mixtures at different ratios are presented and discussed, and the transition from an electropositive to an electronegative discharge is illustrated. It is observed that at high concentration of Ar (90%) the structure of the discharge is similar to that of the electropositive discharge, although some features of electronegative discharges, such as the abundance of negative ions, begin to appear. The Ar⁺ density exceeds the CF₃⁺ density by about 2 orders of magnitude. At equal concentration of Ar and CF₄ the discharge shows more electronegative features. The double layer structure and the electron density maxima in the sheath, which are representative for an electronegative discharge, appear. Electric field reversal is observed as well. However, the major positive ion is still Ar⁺. At high CF₄ concentration the discharge behaves as a typical electronegative discharge and CF₃⁺ is the major positive ion. The results show that the F⁻ ions are the dominant negatively charged species at all Ar/CF₄ ratios investigated.

Finally, the calculated electronegativities in an Ar/CF₄ discharge at a concentration of CF₄ up to 10% over the pressure range from 30 to 100 mTorr are compared with measured data and reasonable agreement is reached.

ACKNOWLEDGMENTS

The authors wish to thank M. Yan for supplying the basic PIC code. V.G. would like to thank K. Denpoh and K. Nanbu for providing their ion-CF₄ reaction data and details of their ion-molecule collision model for endothermic reactions. V.G. and A.B. are indebted to the Flemish Fund for Scientific research (FWO) for financial support. This research is also sponsored by the Federal Services for Scientific, Cultural and Technical Affairs of the Prime Minister's Office through IUAP-V.

¹M. A. Lieberman and A. J. Lichtenberg, *Principles of Plasma Discharges and Materials Processing* (Wiley, New York, 1994).

²B. Chapman, *Glow Discharge Processes* (Wiley, New York, 1980).

³T. Kimura and K. Ohe, *Plasma Sources Sci. Technol.* **8**, 553 (1999).

⁴T. Kimura and K. Ohe, *J. Appl. Phys.* **92**, 1780 (2002).

⁵H. Singh and D. B. Graves, *J. Appl. Phys.* **87**, 4098 (2000).

⁶H. Singh, J. W. Coburn, and D. B. Graves, *J. Vac. Sci. Technol. A* **19**, 718 (2001).

⁷K. Hioki, H. Hirata, S. Matsumura, Z. Lj. Petrovic, and T. Makabe, *J. Vac. Sci. Technol. A* **18**, 864 (2000).

⁸M. D. Bowden, R. Tabata, P. Suanpoot, K. Uchino, K. Muraoka, and M. Noguchi, *J. Appl. Phys.* **90**, 2158 (2001).

⁹K. Maeshige, G. Washio, T. Yagisawa, and T. Makabe, *J. Appl. Phys.* **91**, 9494 (2002).

¹⁰S. Rauf and M. J. Kushner, *J. Appl. Phys.* **82**, 2805 (1997).

¹¹K. Kaga, T. Kimura, T. Imaeda, and K. Ohe, *Jpn. J. Appl. Phys., Part 1* **40**, 6115 (2001).

¹²M. Haverlag, A. Kono, D. Passchier, G. M. W. Kroesen, W. J. Goedheer, and F. J. de Hoog, *J. Appl. Phys.* **70**, 3472 (1991).

¹³J. L. Jauberteau, G. J. Meeusen, M. Haverlag, G. M. W. Kroesen, and F. J. de Hoog, *J. Phys. D* **24**, 261 (1990).

- ¹⁴E. Gogolides, M. Stathakopoulos, and A. Boudouvis, *J. Phys. D* **27**, 1878 (1994).
- ¹⁵N. V. Mantzaris, A. Boudouvis, and E. Gogolides, *J. Appl. Phys.* **77**, 6169 (1991).
- ¹⁶K. Denpoh and K. Nanbu, *J. Vac. Sci. Technol. A* **16**, 1201 (1998).
- ¹⁷E. Gogolides and H. H. Sawin, *J. Appl. Phys.* **72**, 3971 (1992).
- ¹⁸V. Vahedi and M. Surendra, *Comput. Phys. Commun.* **87**, 179 (1995).
- ¹⁹K. Nanbu and Y. Kitatani, *Vacuum* **47**, 1023 (1996).
- ²⁰A. Bogaerts, R. Gijbels, and W. Goedheer, *Jpn. J. Appl. Phys., Part 1* **38**, 4404 (1999).
- ²¹M. Yan, A. Bogaerts, W. J. Goedheer, and R. Gijbels, *Plasma Sources Sci. Technol.* **9**, 583 (2000).
- ²²C. K. Birdsall and A. B. Langdon, *Plasma Physics via Computer Simulation* (McGraw – Hill, New York, 1985).
- ²³E. Kawamura, C. K. Birdsall, and V. Vahedi, *Plasma Sources Sci. Technol.* **9**, 413 (2000).
- ²⁴Ph. Belenguer and J. P. Boeuf, *Phys. Rev. A* **41**, 4447 (1990).
- ²⁵M. Surendra and D. B. Graves, *IEEE Trans. Plasma Sci.* **19**, 144 (1991).
- ²⁶A. Okhrimovskyy, A. Bogaerts, and R. Gijbels, *Phys. Rev. E* **65**, 037402 (2002).
- ²⁷M. Surendra, D. B. Graves, and G. M. Jellum, *Phys. Rev. A* **41**, 1112 (1990).
- ²⁸M. Kurihara, Z. Lj. Petrovic, and T. Makabe, *J. Phys. D* **33**, 2146 (2000).
- ²⁹R. A. Bonham, *Jpn. J. Appl. Phys., Part 1* **33**, 4157 (1994).
- ³⁰K. Denpoh and K. Nanbu (private communication).
- ³¹K. Nanbu and Y. Kitatani, *J. Phys. D* **28**, 324 (1995).
- ³²K. Nanbu and K. Denpoh, *J. Phys. Soc. Jpn.* **67**, 1288 (1998).
- ³³T. Kimura, K. Kaga, and K. Ohe, *Jpn. J. Appl. Phys., Part 1* **39**, 1351 (2000).
- ³⁴K. Denpoh and K. Nanbu, *Jpn. J. Appl. Phys., Part 1* **39**, 2804 (2000).